Received: 21 June 2022 | Revised: 27 September 2022 | Accepted: 14 November 2022

DOI: 10.4218/etrij.2022-0243

ORIGINAL ARTICLE

ETRI Journal WILEY

Channel estimation and detection with space–time transmission scheme in colocated multiple-input and multiple-output system

Pratibha Rani[1] | **Arti M.K.**[2] | **Pradeep Kumar Dimri**[1]

[1]Electronics Engineering, J.C. Bose University of Science and Technology, YMCA, Faridabad, Haryana, India

[2]Electronics and Communications Engineering, Netaji Subhash University of Technology (East Campus), New Delhi, India

Correspondence
Pratibha Rani, Electronics Engineering, J.C. Bose University Of Science and Technology, YMCA, Faridabad, Haryana, India.
Email: pratibhaymca@gmail.com

Abstract

In this study, a space–time transmission scheme is proposed to tackle the limitations of channel estimation with orthogonal pilot information in colocated multiple-input multiple-output systems with several transmitting and receiving antennas. Channel information is obtained using orthogonal pilots. Channel estimation introduces pilot heads required to estimate a channel. This leads to bandwidth insufficiency. As a result, trade-offs exist between the number of pilots required to estimate a channel versus spectral efficiency. The detection of data symbols is performed using the maximum likelihood decoding method as it provides a consistent approach to parameter estimation problems. The moment-generating function of the instantaneous signal-to-noise ratio is used to drive an approximate expression of the symbol error rate for the proposed scheme. Furthermore, the order of diversity is less by one than the number of receiver antennas used in the proposed scheme. The effect of the length of a pilot sequence on the proposed scheme's performance is also investigated.

KEYWORDS

bit error rate, channel estimation, colocated MIMO, diversity order, massive MIMO, pilot length

1 | INTRODUCTION

Conventionally, in wireless communication systems, the term "multiple-input multiple-output (MIMO)" refers to the use of multiple antennas at the transmitter and receiver. In modern usage, "MIMO" pragmatically refers to a practical technique for sending and receiving more than one data signal simultaneously over the same radio channel by exploiting multipath propagation. The term MIMO was first introduced by Brandenburg and Wyner [1], where the information capacity of MIMO channels was derived with memory. Presently, massive MIMO [2–5] is a more focused technique to combat 5^{th} Generation (5G). 5G has emerged as a major factor in health care, artificial intelligence, transport, and so on [6–8]. MIMO wireless systems are part of recent standards worldwide. An overview of the massive MIMO concept and newfangled research has been reported [9]. The massive MIMO technology helps in achieving higher performance in a spatial diversity gain, array gain, interference reduction, and spatial multiplexing gain [10]. The basic difference between massive MIMO and colocated MIMO is that in massive MIMO, communication occurs between users and base station antennas, whereas in colocated MIMO,

communication occurs between the antennas of transmitting and receiving base stations. The massive MIMO technology has facilitated in achieving improved performance in spatial diversity gain, array gain, interference reduction, and spatial multiplexing gain [10]. The combination of colocated MIMO and massive MIMO enhances the capacity of an entire system. This study proposes colocated MIMO with a space–time transmission scheme (STTS), which is less complex than orthogonal space–time block codes [11] used in wireless communication.

Pilots are also known as training symbols [12]. They are used to obtain the channel state information (CSI) of a communication system [13]. Pilot assignment schemes for reducing pilot contamination during channel estimation are categorized into fractional frequency reuse, superimposed pilots, and time shift pilots [14]. In "fractional frequency reuse," pilots are reused with a reuse factor to mitigate the problem of pilot contamination for channel estimation, and this category is also divided into two categories. In the first category, similar cells are allocated similar pilot sequences, whereas other cells are provided with orthogonal pilot sequences. In the second category, users are separated in terms of cell-center and cell-edge users. In this case, pilot contamination severely affects cell-edge users; thus, pilots are reused accordingly. In the fractional frequency reuse method, pilot overhead comes into account, leading to its drawback [15]. In superimposed pilot schemes [16, 17], pilots are transmitted, along with data sequences. This reduces power consumption. The proposed STTS lies under the category of regular orthogonal pilots. In this scheme, there is no pilot overhead. However, there may be interference between pilot and data transmission, which can be diminished with the appropriate amount of power to data and pilots. Channel estimation methods for orthogonal frequency division multiplexing [18] systems based on a comb-type pilot subcarrier arrangement are investigated. The channel estimation algorithm based on comb-type pilots is divided into pilot signal estimation and channel interpolation. The minimum mean square error (MMSE) estimate of pilot signals, inter-carrier interference, and AWGN are reduced significantly. A channel can also be estimated through block-type pilot assignment [19], where all subcarriers are used as pilots. In this case, the complete loss of the estimated channel occurs because of fast fading. Initially, in a comb-type pilot arrangement, the least square error (LSE) estimate is used to obtain CSI [20]. Subsequently, the MMSE is used, which provides better performance than the LSE estimate. However, the MMSE estimate increases the complexity, which is subsequently reduced by driving an optimal low-rank estimator with singular value decomposition. Subsequent channel estimation based on comb-type pilot arrangements through different channel estimation algorithms has been investigated for MIMO in previous studies [21, 22]. Recent advances in massive MIMO focus on providing different approaches to reduce pilot contamination in massive MIMO using pilot assignment schemes. Zhao et al. [19] proposed a cell sectorization-based pilot assignment scheme in which orthogonal pilots are used between adjacent sectors. The results of the scheme show that the scheme could reduce power consumption and achieve high throughput when the number of base station antennas approaches infinity. However, the sum rate is low when the number of antennas is less than 40.

After the review of the literature based on pilot decontamination and pilot allocation, initially, research on pilot assignment methods was based on the frequency reuse method, superimposed pilots, and time shift pilots. However, in recent trends, the allocation of pilots has been performed using deep learning, which involves training a communication system with numerous training samples to estimate CSI [23, 24].

The proposed scheme is compared with space–time block coding over the Rayleigh fading channel. Space–time block coding was introduced for wireless communication systems in [25, 26]. The space–time block code (STBC) is a well-known strategy for MIMO systems to transmit different symbols from different antennas within specific time slots [27]. The encoding of data is performed using STBCs, and then, they are split into s number of streams concurrently transmitted through N_r transmit antennas. The received signal has a linear superposition of s number of transmitted signals with noise at each receiver antenna [25]. With STBCs, multiple copies of a data stream are transmitted to several antennas to improve the reliability and credibility of data transfer. Because of the multiple copies of the received data stream, there may be data very close to the original signal. This data redundancy ensures that the received signal is correctly decoded. STBCs are designed to obtain the maximum diversity order for a given number of transmitting and receiving antennas [27]. Despite the numerous benefits of using orthogonal STBCs (OSTBCs), there are some drawbacks. In most of the existing space–time code designs, maximum likelihood decoding [28, 29] is used to achieve full diversity at the receiver, which is typically computationally expensive and may not have soft outputs. The problem of OSTBC transmission in MIMO systems has been addressed in a previous study [30]. STBCs have the following drawbacks when using numerous antennas, as discussed in the paper [30]: (a) It is difficult to achieve a high data rate in symbol-wise decoding-based STBCs; (b) the decoding complexity is increased with an increase in the data rate in STBCs for large dimensions; (c) OSTBCs are designed under the

restriction of full diversity, which is very significant in the case of massive MIMO, which is practically not required; (d) STBCs require a large coherence time. OSTBCs compromise the data rate for high spatial dimensions, whereas nonorthogonal STBCs sacrifice decoupled decoding. In this study, STTS has been proposed for colocated MIMO communication from transmitting base station antennas to receiving base station antennas. The scheme is less complex than OSTBCs for large dimensions. In the proposed scheme, pilot symbol vectors and data vectors are placed in space and time dimensions in a data transmission matrix. Pilot sequences are adequate resources as the length of a pilot sequence is limited by the coherence bandwidth of the channel and coherence time. The interference between pilot symbols or sequences is known as pilot contamination [31–33]. However, in colocated MIMO, such interference during communication does not exist. For simplicity, orthogonal pilot vectors are used in the proposed scheme. In the proposed scheme, the detection of data symbols is performed through maximum likelihood detection with the help of estimated CSI. The concept of space null is used to obtain the estimated channel information. The moment-generating function (MGF) [34–36] is used to derive the expression of bit error rate (BER) [37–39]. The performance of the system is observed with the variable length of pilot sequences. The expression of the diversity order and its plot are obtained.

2 | SYSTEM MODEL AND PILOT-BASED STTS

As depicted in Figure 1, the tiny holes represent a large number of antennas $N_1, N_2, N_3, ..., N_t$ at the transmitter T_x and $N_1, N_2, N_3, ..., N_r$ at the receiver R_x. Transmission occurs from various antennas of T_x to R_x in the time division duplex (TDD) approach. The wireless channel between T_x and R_x is represented by $\mathbf{H}$. The entries of the channel matrix, $\mathbf{H}$, are complex Gaussian with unit variance and zero mean. The noise, $\mathbf{G}$, during communication is considered as AWGN with σ^2 variance and zero mean.

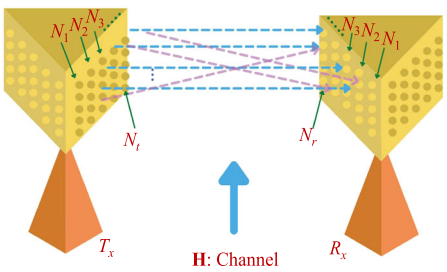

FIGURE 1 System model.

2.1 | STTS

The positions of pilot and data vectors in STTS are shown in Figure 2. The vertical direction represents the transmission in the spatial domain (i.e., according to the number of transmitting antennas), and the horizontal direction represents the transmission in the time slots. Four transmitting and receiving antennas are considered with the TDD approach for clarity in the proposed scheme.

Data symbol vectors are transmitted, along with pilot symbol vectors. The length of a pilot vector is directly proportional to the length of a data vector. A minimum of four time slots are required to transmit data from four transmitting antennas. Thus, $\mathbf{D} \in \mathbb{C}^{4\times 16}$ represents the transmission matrix of a data vector, $\mathbf{d}_{ij}(s), i \in \{1,...,4\}$ and $j \in \{1,...,4\}$ for $N_t = 4$ and $N_r = 4$. Pilot symbol vector, $\boldsymbol{\rho}_{ij}(s), i \in \{1,...,4\}$. Data vectors are the vectors of symbols from the M-PSK constellation, and $\boldsymbol{\rho}_{ij}(s)$ are orthogonal pilot sequences, that is, the product of one pilot vector with any other pilot vector gives a zero value (Null value), and $|\rho_{ij}|^2 = 1$.

$$\mathbf{D} = \begin{bmatrix} \mathbf{D}_{11} & \mathbf{D}_{12} & \mathbf{D}_{13} & \mathbf{D}_{14} \\ \mathbf{D}_{21} & \mathbf{D}_{22} & \mathbf{D}_{23} & \mathbf{D}_{24} \\ \mathbf{D}_{31} & \mathbf{D}_{32} & \mathbf{D}_{33} & \mathbf{D}_{34} \\ \mathbf{D}_{41} & \mathbf{D}_{42} & \mathbf{D}_{43} & \mathbf{D}_{44} \end{bmatrix} = \begin{bmatrix} \boldsymbol{\rho}_{11} & \mathbf{d}_{12} & \boldsymbol{\rho}_{13} & \mathbf{d}_{14} \\ \boldsymbol{\rho}_{21} & -\mathbf{d}_{22} & \boldsymbol{\rho}_{23} & -\mathbf{d}_{24} \\ \mathbf{d}_{31} & \boldsymbol{\rho}_{32} & \mathbf{d}_{33} & \boldsymbol{\rho}_{34} \\ -\mathbf{d}_{41} & \boldsymbol{\rho}_{42} & -\mathbf{d}_{43} & \boldsymbol{\rho}_{44} \end{bmatrix}. \quad (1)$$

In (1), rows denote the transmission of pilot and data symbol vectors from the respective transmitting antennas. $\mathbf{D}_{mn}(s)$ represent the vector, where m represents data from the transmitting antenna, and n

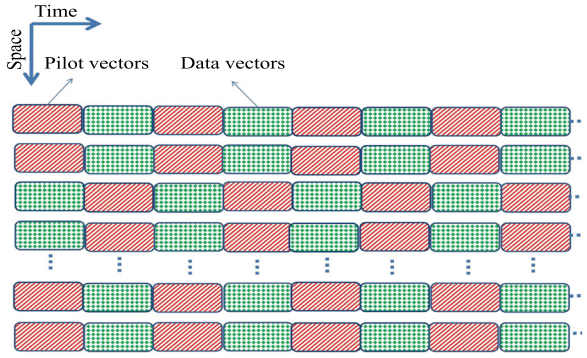

FIGURE 2 Positions of pilot and data vectors.

represents the time slot. Here, $\mathbf{D}_{11}(s)$, where $m=1$ and $n=1$, represents the pilot symbol vector from the first transmitting antenna in the first time slot. $\mathbf{D}_{12}(s)$, where $m=1$ and $n=2$, represents the data symbol vector from the first antenna in the second time slot. $\mathbf{D}_{13}(s)$, where $m=1$ and $n=3$, represents the pilot symbol vector from the first transmitting antenna in the third time slot. $\mathbf{D}_{14}(s)$, where $m=1$ and $n=4$, represents the data symbol vector from the first antenna in the fourth time slot. Furthermore, $\mathbf{D}_{21}(s)$, where $m=2$ and $n=1$, represents the pilot symbol vector from the second transmitting antenna in the first time slot. $\mathbf{D}_{22}(s)$, where $m=2$ and $n=2$, represents the negative of the same data symbol vector from the second transmitting antenna in the second time slot. $\mathbf{D}_{23}(s)$, where $m=2$ and $n=3$, represents the pilot symbol vector from the second transmitting antenna in the third time slot. $\mathbf{D}_{24}(s)$, where $m=2$ and $n=4$, represents the data symbol vector from the second transmitting antenna in the fourth time slot. The third and fourth rows of the transmission data matrix are similar, except that the data symbol vectors in the fourth row are negative. Intuitively, that communication along the row represents communication in the time domain or time slots, and communication along the column represents communication in the frequency (space) domain with different transmission antennas. The transmission matrix extends as the number of antennas or time slots increases. The received signal is given by

$$\mathbf{Z}=\mathbf{HD}+\mathbf{G}, \tag{2}$$

where $\mathbf{H} \in \mathbb{C}^{N_r \times N_t}$ $\mathbb{C}$ is a set of complex numbers and is the channel matrix of a large MIMO system between the receiver and transmitter. AWGN with σ^2 variance and zero mean is represented by $\mathbf{G}$. In a practical framework, channel information is unknown. However, channel information is required to receive a data signal. Therefore, the first task is to obtain CSI using known pilot symbol vectors at the transmitting and receiving ends. According to (1) and (2), a received signal can be expressed as

The generalized equation under the scheme is as follows:

$$\begin{aligned}[\mathbf{Z}_1\ \mathbf{Z}_2\ \ldots\ \mathbf{Z}_\theta] &= [\mathbf{h}_1\ \mathbf{h}_2\ \ldots\ \mathbf{h}_\theta] \\ &\times \begin{bmatrix} \boldsymbol{\rho}_{11} & \mathbf{d}_{12} & \boldsymbol{\rho}_{13} & \mathbf{d}_{14} & \ldots & \mathbf{d}_{1j} \\ \boldsymbol{\rho}_{21} & -\mathbf{d}_{22} & \boldsymbol{\rho}_{23} & -\mathbf{d}_{24} & \ldots & \mathbf{d}_{2j} \\ \mathbf{d}_{31} & \boldsymbol{\rho}_{32} & \mathbf{d}_{33} & \boldsymbol{\rho}_{34} & \ldots & \mathbf{d}_{3j} \\ -\mathbf{d}_{41} & \boldsymbol{\rho}_{42} & -\mathbf{d}_{43} & \boldsymbol{\rho}_{44} & \ldots & \mathbf{d}_{4j} \\ \vdots & \vdots & \vdots & \vdots & \ldots & \vdots \\ -\mathbf{d}_{i1} & \boldsymbol{\rho}_{i2} & -\mathbf{d}_{i3} & \boldsymbol{\rho}_{i4} & \ldots & \mathbf{d}_{ij} \end{bmatrix} \\ &+[\mathbf{G}_1\ \mathbf{G}_2\ \ldots\ \mathbf{G}_\theta], \end{aligned} \tag{3}$$

where, in (3), $Z_\theta \in \mathbb{C}^{L\times j}, h_\theta = [h_{1t}h_{2t}h_{3t}\cdots h_{rt}]^{\mathrm{T}} \in \mathbb{C}^{N_r\times 1}$ in which h_θ represents the column vector in the channel matrix, t represents the number of transmitting antennas, $r=\{1,2,3,...,N_r\}$, j represents the number of time slots, $(.)^{\mathrm{T}}$ represents the matrix transpose, and L represents the length of the pilot sequence. The complete received signal matrix, channel matrix, and noise matrix for variables N_t and N_r are

$$\mathbf{Z}=[\mathbf{Z}_1\ \ \mathbf{Z}_2\ \ \mathbf{Z}_3\ldots\ \ \mathbf{Z}_\theta] \in \mathbb{C}^{N_r\times(N_r\times N_r)}, \tag{4}$$

$$\mathbf{H}=[\mathbf{h}_1\ \ \mathbf{h}_2\ \ \mathbf{h}_3\ldots\ \ \mathbf{h}_\theta] \in \mathbb{C}^{N_r\times N_t}, \tag{5}$$

and

$$\mathbf{G}=[\mathbf{G_1}\ \ \mathbf{G_2}\ \ \mathbf{G_3}\ \ \ldots\ \ \mathbf{G_\theta}] \in \mathbb{C}^{N_r\times(N_r\times N_r)}), \tag{6}$$

where $\mathbf{Z}_k \in \mathbb{C}^{4\times 4}, \mathbf{k} \in \{1,\ldots,4\}$ and $\mathbf{h}_i = [h_{i_1}\ \ h_{i_2}\ \ h_{i_3}\ \ h_{i_4}]^{\mathrm{T}}$ $\mathbb{C}^{4\times 1}$. $\mathbf{G}_k \in \mathbb{C}^{4\times 4}$ are complex valued Gaussian noise matrixes.

From (3), the elaborate representation for (4×4) system leads to

$$\mathbf{Z}_1=\mathbf{h}_1\boldsymbol{\rho}_1+\mathbf{h}_2\mathbf{d}_1+\mathbf{h}_3\boldsymbol{\rho}_2+\mathbf{h}_4\mathbf{d}_2+\mathbf{G}_1, \tag{7}$$

$$\mathbf{Z}_2=\mathbf{h}_1\boldsymbol{\rho}_1-\mathbf{h}_2\mathbf{d}_1+\mathbf{h}_3\boldsymbol{\rho}_2-\mathbf{h}_4\mathbf{d}_2+\mathbf{G}_2, \tag{8}$$

$$\mathbf{Z}_3=\mathbf{h}_1\mathbf{d}_3+\mathbf{h}_2\boldsymbol{\rho}_3+\mathbf{h}_3\mathbf{d}_4+\mathbf{h}_4\boldsymbol{\rho}_4+\mathbf{G}_3, \tag{9}$$

$$\mathbf{Z}_4=-\mathbf{h}_1\mathbf{d}_3+\mathbf{h}_2\boldsymbol{\rho}_3-\mathbf{h}_3\mathbf{d}_4+\mathbf{h}_4\boldsymbol{\rho}_4+\mathbf{G}_4. \tag{10}$$

Because channel entries are not available at the receiving end which in turn will not allow the recovery of the transmitted data symbols. Adding (7) and (8) produces entries of the channel $\mathbf{h}_1$ and $\mathbf{h}_3$, resulting in

$$\frac{\mathbf{Z}_1+\mathbf{Z}_2}{2}=\mathbf{h}_1\boldsymbol{\rho}_1+\mathbf{h}_3\boldsymbol{\rho}_2+\frac{\mathbf{G}_1+\mathbf{G}_2}{2}. \tag{11}$$

Pilot symbol vectors are known at both the transmitting and receiving ends. All pilot vectors are orthogonal to each other [9]. Utilizing this property of the pilots, we obtain the entries of $\mathbf{h}_1$. Equation (11) is multiplied with the hermitian of $\boldsymbol{\rho}_1$, which yields

$$\left(\frac{\mathbf{Z}_1+\mathbf{Z}_2}{2}\right)\rho_1^{\mathrm{H}}=\mathbf{h}_1+\left(\frac{\mathbf{G}_1+\mathbf{G}_2}{2}\right)\rho_1^{\mathrm{H}}=\hat{\mathbf{h}}_1. \tag{12}$$

In (8), $\rho_1{\rho_1}^{\mathrm{H}}$=1, where $(.)^{\mathrm{H}}$ is the conjugate transpose, and $\rho_2{\rho_1}^{\mathrm{H}}=0$ from the property of orthogonality.

The estimated channel vector of the first transmitting antenna to all receiving antennas is given by $\hat{\mathbf{h}}_1$. Likewise, we can obtain $\mathbf{h}_3$ from (11), $\mathbf{h}_2$, and $\mathbf{h}_4$ after applying the same procedure as (9) and (10). The estimated channel matrix is

$$\mathbf{H} = \left[\hat{\mathbf{h}}_1 \;\; \hat{\mathbf{h}}_2 \;\; \hat{\mathbf{h}}_3 \;\; \hat{\mathbf{h}}_4\right], \tag{13}$$

where $\hat{\mathbf{h}}_2, \hat{\mathbf{h}}_3$, and $\hat{\mathbf{h}}_4$ represent the estimated channel vectors of $\mathbf{N}_2, \mathbf{N}_3$, and $\mathbf{N}_4$ transmitting antennas, respectively.

2.2 | Signal recognition

Signal detection or recognition is the ability of a system to differentiate between transmitted information patterns and random patterns. Signal detection under the proposed scheme is performed using estimated channel gains at the receiver. The difference between (7) and (8) produces

$$\frac{\mathbf{Z}_1 - \mathbf{Z}_2}{2} = \mathbf{h}_2\mathbf{d}_1 + \mathbf{h}_4\mathbf{d}_2 + \frac{\mathbf{G}_1 - \mathbf{G}_2}{2}. \tag{14}$$

In (14), $\mathbf{d}_1$ and $\mathbf{d}_2$ represent the transmitted symbol vector from $\mathbf{N}_1$ in different time slots. Therefore, to detect $\mathbf{d}_1$, the effect of $\mathbf{d}_2$ is to be neutralized.

To achieve the same result, the entire term is multiplied by the left null of $\mathbf{h}_4$. After nulling, it is observed through simulation that the left null of a column vector with more than two elements is a matrix [12, 40]. The nulling matrix is $\mathbf{F}_4 = (\text{null}(\hat{\mathbf{h}}_4^{\text{H}}))^{\text{H}}$. Then, the equation becomes

$$\mathbf{F}_4\left(\frac{\mathbf{Z}_1 - \mathbf{Z}_2}{2}\right) = \mathbf{F}_4\mathbf{h}_2\mathbf{d}_1 + \underbrace{\mathbf{F}_4\mathbf{h}_4\mathbf{d}_2}_{0} + \mathbf{F}_4\left(\frac{\mathbf{G}_1 - \mathbf{G}_2}{2}\right). \tag{15}$$

Because $\mathbf{F}_4\mathbf{h}_4 \simeq 0$ from property of space null, (15) transforms into

$$\mathbf{F}_4\left(\frac{\mathbf{Z}_1 - \mathbf{Z}_2}{2}\right) = \mathbf{F}_4\mathbf{h}_2\mathbf{d}_1 + \mathbf{F}_4\left(\frac{\mathbf{G}_1 - \mathbf{G}_2}{2}\right). \tag{16}$$

In (16), noise needs to be eliminated for perfect signal detection. Therefore, whitening of noise is performed, resulting in

$$\begin{aligned}\delta_1 &= \mathbf{E}_1^{\left(-\frac{1}{2}\right)}\mathbf{F}_4\left(\frac{\mathbf{Z}_1 - \mathbf{Z}_2}{2}\right)\\ &= \mathbf{E}_1^{\left(-\frac{1}{2}\right)}\mathbf{F}_4\mathbf{h}_2\mathbf{d}_1 + \mathbf{E}_1^{\left(-\frac{1}{2}\right)}t_1,\end{aligned} \tag{17}$$

where $t_1 = \mathbf{F}_4((\mathbf{G}_1 - \mathbf{G}_2)/\ (2))$. In (17), t_1 is the AWGN matrix that has unit variance and zero mean; that is, it has a normal distribution in the time domain with an average time domain value of zero and has a uniform distribution of power across the frequency band of the information system. Consider $\omega_1 = \mathbf{E}_1^{(-1/2)}t_1$. The whitening of the noiseterm gives, $\mathbf{E}_1 = \text{E}\left(\mathbf{F}_4((\mathbf{G}_1 - \mathbf{G}_2)/(2))\mathbf{F}_4((\mathbf{G}_1 - \mathbf{G}_2)/(2))^{\text{H}}\right)$. E(.) denotes the expectation operator. $\mathbf{E}_1 = \frac{\sigma^2}{2}\mathbf{I}$ because through simulation, it is obtained that $\mathbf{F}_4\mathbf{F}_4^{\text{H}} = \mathbf{I}$, where $\mathbf{I}$ denotes the identity matrix. For $N_t = 4$ and $N_r = 4$, the size of the null matrix is 3×4 as nulling decreases the size of the matrix by one [12, 40]. The maximum likelihood detection of $\mathbf{d}_1$ is obtained by maximizing the conditional probability density function (PDF) of the δ_1 condition on $\mathbf{F}_4$ and $\mathbf{h}_2$. Thus,

$$\hat{\mathbf{d}}_1 = \arg\min_{\tilde{\mathbf{d}}_1} \|\delta_1 - \mathbf{E}_1^{\left(-\frac{1}{2}\right)}\mathbf{F}_4\mathbf{h}_2\tilde{\mathbf{d}}_1\|^2. \tag{18}$$

Similarly, the other data values can be obtained from

$$\hat{\mathbf{d}}_2 = \arg\min_{\tilde{\mathbf{d}}_2} \|\delta_2 - \mathbf{E}_2^{\left(-\frac{1}{2}\right)}\mathbf{F}_2\mathbf{h}_4\tilde{\mathbf{d}}_2\|^2, \tag{19}$$

$$\hat{\mathbf{d}}_3 = \arg\min_{\tilde{\mathbf{d}}_3} \|\delta_3 - \mathbf{E}_3^{\left(-\frac{1}{2}\right)}\mathbf{F}_3\mathbf{h}_1\tilde{\mathbf{d}}_3\|^2, \tag{20}$$

$$\hat{\mathbf{d}}_4 = \arg\min_{\tilde{\mathbf{d}}_4} \|\delta_4 - \mathbf{E}_4^{\left(-\frac{1}{2}\right)}\mathbf{F}_1\mathbf{h}_3\tilde{\mathbf{d}}_4\|^2, \tag{21}$$

where $\delta_1 = \delta_2 = ((\mathbf{Z}_1 - \mathbf{Z}_2)/2)$, $\delta_3 = \delta_4 = ((\mathbf{Z}_3 - \mathbf{Z}_4)/2)$, $\mathbf{E}_1 = \mathbf{E}_2 = \mathbf{E}_3 = \mathbf{E}_4 = \frac{\sigma^2}{2}\mathbf{I}, \mathbf{F}_i = (\text{null}(\hat{\mathbf{h}}_i^{\text{H}}))^{\text{H}}$, and $i = 1, 2, 3$, and 4 for $N_r = 4$ and $N_t = 4$.

3 | PERFORMANCE ANALYSIS

The performance analysis of the proposed STTS-based system is performed in terms of the error probability and diversity gain [41].

3.1 | Expression of instantaneous signal-to-noise ratio (SNR)

The SNR is the measure of signal quality and is given as

$$S_{\text{n}} = \frac{S_{\text{p}}}{N_{\text{p}}}, \tag{22}$$

where S_n, S_p, and N_p represent the SNR, signal power, and noise power, respectively. The SNR in dB is given as

$$[S_n]_{dB} = 10\log_{10}\left(\frac{S_p}{N_p}\right). \tag{23}$$

The instantaneous value of the received SNR for the first transmitted symbol vector is calculated. As the channel is not known at the receiver, the estimated channel is considered, and (18) becomes

$$\hat{\mathbf{d}}_1 = \arg\min_{\tilde{\mathbf{d}}_1} \|\delta_1 - \mathbf{E}_1^{\left(-\frac{1}{2}\right)}\hat{\mathbf{F}}_4\hat{\mathbf{h}}_2\tilde{\mathbf{d}}_1\|^2. \tag{24}$$

After putting the value of δ_1, we obtain

$$\hat{\mathbf{d}}_1 = \arg\min_{\tilde{\mathbf{d}}_1} \|\mathbf{E}_1^{\left(-\frac{1}{2}\right)}\mathbf{F}_4\mathbf{h}_2\mathbf{d}_1 + \omega_1 - \mathbf{E}_1^{\left(-\frac{1}{2}\right)}\hat{\mathbf{F}}_4\hat{\mathbf{h}}_2\tilde{\mathbf{d}}_1\|^2. \tag{25}$$

The value of $\mathbf{F}_4$ is

$$\begin{aligned}\hat{\mathbf{F}}_4 = \text{null}\left(\hat{\mathbf{h}}_4^{\text{H}}\right) &= \text{null}\left(\mathbf{h}_4 + \left(\frac{\mathbf{G}_3+\mathbf{G}_4}{2}\right)\rho_4^{\text{H}}\right)^{\text{H}} \\ &= \text{null}\quad \mathbf{h}_4^{\text{H}} + \rho_4\left(\frac{\mathbf{G}_3+\mathbf{G}_4}{2}\right)^{\text{H}}\Bigg) \\ &= \text{null}\left(\mathbf{h}_4^{\text{H}}\right) + \underbrace{\text{null}\left(\rho_4\left(\frac{\mathbf{G}_3+\mathbf{G}_4}{2}\right)^{\text{H}}\right)}_{\eta_4}.\end{aligned} \tag{26}$$

Then, the equation becomes

$$\hat{\mathbf{F}}_4 = \mathbf{F}_4 + \eta_4. \tag{27}$$

In (27), η_4 represent noise. Using (9) and (10), we obtain $\hat{\mathbf{h}}_2$ as

$$\hat{\mathbf{h}}_2 = \mathbf{h}_2 + \left(\frac{\mathbf{G}_3+\mathbf{G}_4}{2}\right)\rho_3^{\text{H}} = \mathbf{h}_2 + \mathbf{n}_e\rho_3^{\text{H}}, \tag{28}$$

where $\mathbf{n}_e = ((\mathbf{G}_3+\mathbf{G}_4)/2)$. Then, after inputting the value of $\hat{\mathbf{h}}_2^{\text{H}}$ and $\hat{\mathbf{F}}_4^{\text{H}}$ in (25), we obtain

$$\begin{aligned}\hat{\mathbf{d}}_1 &= \arg\min_{\tilde{\mathbf{d}}_1} \|\mathbf{E}_1^{\left(-\frac{1}{2}\right)}\mathbf{F}_4\mathbf{h}_2\mathbf{d}_1 + \omega_1 \\ &\quad -\mathbf{E}_1^{\left(-\frac{1}{2}\right)}(\mathbf{F}_4+\eta_4)(\mathbf{h}_2+\mathbf{n}_e\rho_3^{\text{H}})\tilde{\mathbf{d}}_1\|^2,\end{aligned}$$

$$\begin{aligned}\hat{\mathbf{d}}_1 &= \arg\min_{\tilde{\mathbf{d}}_1} \|\mathbf{E}_1^{\left(-\frac{1}{2}\right)}\mathbf{F}_4\mathbf{h}_2\mathbf{d}_1 + \omega_1 - \mathbf{E}_1^{\left(-\frac{1}{2}\right)}\mathbf{F}_4\mathbf{h}_2\tilde{\mathbf{d}}_1 \\ &\quad -\mathbf{E}_1^{\left(-\frac{1}{2}\right)}\mathbf{F}_4\mathbf{n}_e\rho_3^{H}\tilde{\mathbf{d}}_1 - \mathbf{E}_1^{\left(-\frac{1}{2}\right)}\eta_4\mathbf{h}_2\tilde{\mathbf{d}}_1 - \mathbf{E}_1^{\left(-\frac{1}{2}\right)}\eta_4\mathbf{n}_e\rho_3^{H}\tilde{\mathbf{d}}_1\|^2,\end{aligned} \tag{29}$$

In (29), the term $\mathbf{E}_1^{(-1/2)}\eta_4\mathbf{n}_e\rho_3^{\text{H}}\tilde{\mathbf{d}}_1 = 0$ as the term contain higher order noise. Then, (29) becomes

$$\begin{aligned}\hat{\mathbf{d}}_1 = \arg\min_{\tilde{\mathbf{d}}_1} \|&\underbrace{\mathbf{E}_1^{\left(-\frac{1}{2}\right)}\mathbf{F}_4\mathbf{h}_2\mathbf{d}_1}_{\text{first term}} + \underbrace{\omega_1}_{\text{second term}} \underbrace{-\mathbf{E}_1^{\left(-\frac{1}{2}\right)}\mathbf{F}_4\mathbf{h}_2\tilde{\mathbf{d}}_1}_{\text{third term}} \\ &\underbrace{-\mathbf{E}_1^{\left(-\frac{1}{2}\right)}\mathbf{F}_4\mathbf{n}_e\rho_3^{\text{H}}\tilde{\mathbf{d}}_1}_{\text{fourth term}} \underbrace{-\mathbf{E}_1^{\left(-\frac{1}{2}\right)}\eta_4\mathbf{h}_2\tilde{\mathbf{d}}_1}_{\text{fifth term}}\|^2.\end{aligned} \tag{30}$$

Noise and channel coefficients are assumed to be independent. Thus, the fifth term is neglected. Hence, for simplicity, (30) becomes

$$\begin{aligned}\hat{\mathbf{d}}_1 = \arg\min_{\tilde{\mathbf{d}}_1} \|&\mathbf{E}_1^{\left(-\frac{1}{2}\right)}\mathbf{F}_4\mathbf{h}_2(\mathbf{d}_1-\tilde{\mathbf{d}}_1) + \omega_1 \\ &-\mathbf{E}_1^{\left(-\frac{1}{2}\right)}\mathbf{F}_4\mathbf{n}_e\rho_3^{\text{H}}\tilde{\mathbf{d}}_1\|^2.\end{aligned}$$

$$\hat{\mathbf{d}}_1 = \underbrace{\|\mathbf{E}_1^{\left(-\frac{1}{2}\right)}\mathbf{F}_4\mathbf{h}_2(\mathbf{d}_1-\tilde{\mathbf{d}}_1)\|^2}_{\text{Signal power}} + \|\omega_1\|^2 - \|\mathbf{E}_1^{\left(-\frac{1}{2}\right)}\mathbf{F}_4\mathbf{n}_e\rho_3^{\text{H}}\tilde{\mathbf{d}}_1\|^2. \tag{31}$$

The first term in (31) represents the signal power, and the remaining terms collectively represent noise power. Hence, the signal power and noise power are mentioned below as,

$$S_p = \frac{2}{\sigma^2}\|\mathbf{F}_4\mathbf{h}_2(\mathbf{d}_1-\tilde{\mathbf{d}}_1)\|^2, \tag{32a}$$

$$N_p = \|\omega_1\|^2 - \|\mathbf{E}_1^{\left(-\frac{1}{2}\right)}\mathbf{F}_4\mathbf{n}_e\rho_3^{\text{H}}\tilde{\mathbf{d}}_1\|^2. \tag{32b}$$

Here, $\omega_1 = \mathbf{E}_1^{(-1/2)}\mathbf{F}_4((\mathbf{G}_1-\mathbf{G}_2)/2)$. After solving the term, we obtain $\|\omega_1\|^2$ as constant. For simplicity, we consider $\|\omega_1\|^2$ as 2, and the noise power becomes

$$N_p = 2 - \left(\mathbf{E}_1^{\left(-\frac{1}{2}\right)}\mathbf{F}_4\mathbf{n}_e\rho_3^{\text{H}}\tilde{\mathbf{d}}_1\right)\left(\mathbf{E}_1^{\left(-\frac{1}{2}\right)}\mathbf{F}_4\mathbf{n}_e\rho_3^{\text{H}}\tilde{\mathbf{d}}_1\right)^{\text{H}}. \tag{33}$$

Because $\mathbf{E}_1^{\left(-\frac{1}{2}\right)} * \mathbf{E}_1^{\left(-\frac{1}{2}\right)\mathrm{H}} = \frac{2}{\sigma^2}$, $\mathbf{F}_4 * \mathbf{F}_4^{\mathrm{H}} = \mathbf{I}$, $\mathbf{n}_e * \mathbf{n}_e^{\mathrm{H}} = \sigma^2$, $\eta_4 * \eta_4^{\mathrm{H}} = \sigma^2$, and $\mathbf{d}_1 * \tilde{\mathbf{d}}_1^{H} = 1$, the noise power becomes

$$N_p = 2 - 2\|\boldsymbol{\rho}_3\|^2. \tag{34}$$

Using (32a) and (34), we obtain the instantaneous SNR μ_1 corresponding to data symbol as

$$\mu_1 = \frac{\frac{2}{\sigma^2}\|\mathbf{F}_4\mathbf{h}_2(\mathbf{d}_1 - \tilde{\mathbf{d}}_1)\|^2}{2 - 2\|\boldsymbol{\rho}_3\|^2},$$

$$\mu_1 = \frac{\mathrm{E}|\mathbf{d}_1 - \tilde{\mathbf{d}}_1|^2\|\mathbf{F}_4\mathbf{h}_2\|^2}{\sigma^2\left(1 - \|\boldsymbol{\rho}_3\|^2\right)}, \tag{35}$$

$$\mu_1 = \overline{\mu}_1 * \alpha$$

where

$$\overline{\mu}_1 = \text{Average SNR} = \frac{\mathbf{E}|\mathbf{d}_1 - \tilde{\mathbf{d}}_1|^2}{\sigma^2}$$

and

$$\alpha = \frac{\|\mathbf{F}_4\mathbf{h}_2\|^2}{1 - \|\boldsymbol{\rho}_3\|^2}.$$

Now, the generalized average SNR becomes

$$\overline{\mu}_i = \frac{\mathrm{E}|\mathbf{d}_i - \tilde{\mathbf{d}}_i|^2}{\sigma^2}. \tag{36}$$

Note that $i = 1$, 2, 3, and 4 in the considered case. μ_1 denotes the SNR of the first transmitted symbol vector. Now, α is

$$\alpha = \upsilon * \tau,$$

where

$$\upsilon = \frac{1}{1 - \|\boldsymbol{\rho}_3\|^2}$$

and

$$\tau = \|\mathbf{F}_4\mathbf{h}_2\|^2.$$

The term $\|\boldsymbol{\rho}_3\|^2$ is considered an average, that is, $(\sum_{j=1}^{L}|\boldsymbol{\rho}_{3j}|^2)/L$, where $j = 1$, 2, 3, ..., L, and L represents the length of the pilot. Now, υ becomes

$$\upsilon = \frac{1}{1 - \frac{\sum_{j=1}^{L}|\boldsymbol{\rho}_{3j}|^2}{L}}$$

$$\upsilon = \sum_{m=0}^{\infty}\left(\frac{\sum_{j=1}^{L}|\boldsymbol{\rho}_{3j}|^2}{L}\right)^m, \tag{37}$$

where (37) is the maclaurin expansion [42] of the term υ in which $(\sum_{j=1}^{L}|\boldsymbol{\rho}_{3j}|^2)/L < 1$.

3.2 | Moment-generating function

The expression of the MGF is obtained using the singular value decomposition [12, 40] of the obtained matrix $\mathbf{F}$. The decomposition of $\mathbf{F}$ is as follows:

$$\|\mathbf{F}_4\mathbf{h}_2\|^2 = \|\mathbf{VQR}^{\mathrm{H}}\mathbf{h}_2\|^2 = \|\mathbf{VQ}\tilde{\mathbf{h}}_2\|^2, \tag{38}$$

where $\mathbf{Q}$ represents a diagonal matrix, and $\mathbf{V}$ and $\mathbf{R}$ represent unitary matrices. The value of $\tilde{\mathbf{h}}_2 = \mathbf{R}^{\mathrm{H}}\mathbf{h}_2$. Here, $\tilde{\mathbf{h}}_2$ has the same distribution as $\mathbf{h}_2$, which is circularly symmetric complex Gaussian, and $\mathbf{R}$ represents a unitary matrix. $\mathbf{V}^{\mathrm{H}}\mathbf{V} = I$.

Now,

$$\|\mathbf{VQ}\tilde{\mathbf{h}}_2\|^2 = \|\mathbf{Q}\tilde{\mathbf{h}}\|^2 = \sum_{i=1}^{N_r-1}\Lambda_i^2\|\tilde{\mathbf{h}}_{2i}\|^2, \tag{39}$$

where Λ_i are the eigenvalues, $i = 1,2,3$ ..., N_r, and $\tilde{\mathbf{h}}_{2i}$ are the complex values of the channel from transmitter 2 to N_r.

From (39) and (35), we obtain

$$\mu_i = \sum_{i=1}^{N_r-1}|\tilde{\mathbf{h}}_{2i}|^2\sum_{m=0}^{\infty}\left(\frac{\sum_{j=1}^{L}|\boldsymbol{\rho}_{3j}|^2}{L}\right)^m\overline{\mu}_i, \tag{40}$$

$$\mu_i = \sum_{i=1}^{N_r-1}|\tilde{\mathbf{h}}_{2i}|^2 * \upsilon * \overline{\mu}_i.$$

All channel coefficients are Gaussian distributed with unit variance and zero mean. Therefore, the distribution of $\sum_{i=1}^{N_r-1}|\tilde{\mathbf{h}}_{2i}|^2$ is a central chi-square with $2(N_r - 1)$ degree of freedom. The probability distribution of the random variable x is given by [35]

$$P_x(x) = \frac{1}{2^{\frac{m}{2}}\Gamma(\frac{m}{2})\sigma^m}x^{(\frac{m}{2}-1)}\exp(\frac{x}{2\sigma^2}) \quad \text{for } x > 0, \tag{41}$$

where $\Gamma(m/2)$ represents a gamma function, which has close form values for the integer m. Similarly, the PDF of $\sum_{i=1}^{N_r-1}|\tilde{\mathbf{h}}_{2i}|^2$ can be written as

$$P_b(b) = \frac{b^{N_r-2}\exp(-\frac{b}{2\sigma^2})}{2^{N_r-1}(\Gamma(N_r-1)\sigma^{2(N_r-1)}}. \tag{42}$$

In (41), σ is neglected as it is minute. Thus, the equation becomes

$$P_b(b) = \frac{b^{N_r-2}\exp(-\frac{b}{2\sigma^2})}{2^{N_r-1}\Gamma(N_r-1)}. \tag{43}$$

Furthermore, the MGF is obtained as

$$M_{\mu_i}(s) \triangleq \int_0^{\infty} \exp(-sb\mu_i)P_b(b)db, \tag{44}$$

from (40) and (41)

$$M_{\mu_i}(s) \triangleq \int_0^{\infty} \exp(-sb\upsilon\overline{\mu}_i)\frac{b^{N_r-2}\exp(-\frac{b}{2\sigma^2})}{2^{N_r-1}\Gamma(N_r-1)}da. \tag{45}$$

After comparing the integral with the equation in Gradshteyn [42], that is, 3.381.7, we obtain

$$M_{\mu_i}(s) \triangleq \frac{1}{(1+2sb\upsilon\overline{\mu}_i)^{N_r-1}}. \tag{46}$$

3.3 | Expression of symbol error rate (SER)

The MGF aids in obtaining the expression of the SER, which can be calculated using the relation:

$$Q_K = \frac{1}{\pi}\int_0^{M} M_{\mu_i}\left(\frac{K}{\sin^2\theta}\right)d\theta, \tag{47}$$

where $_M = \pi(M-1)/M$ and $K = \sin^2(\pi/M)$, and the approximated value of (44) can be written, as in Simon and Alouini [43],

$$Q_K \approx \sum_{s=1}^{3}\psi_s M_{\mu_i}(\xi_s), \tag{48}$$

where $\psi_1 = (\theta_M/2\pi) - (1/6), \psi_2 = 1/4, \psi_3 = (\theta_M/2\pi) - (1/4), \xi_1 = K, \xi_2 = (4K/3)$, and $\xi_3 = K/\sin^2(\theta_M)$

An approximate value of SER can be obtained using (46) and (48),

$$Q_K \approx \sum_{s=1}^{3}\frac{\psi_s}{(1+\psi_s\upsilon\mu_i)^{(N_r-1)}}. \tag{49}$$

Equation (49) shows that the SER is inversely proportional to the length of the pilot sequences.

3.4 | Expression of diversity order

When a signal is transmitted through independent channels, fading occurs, making perfect signal recovery

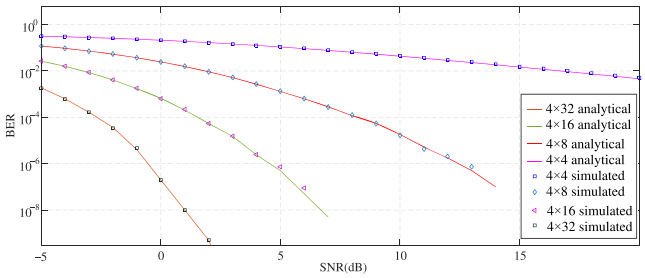

FIGURE 3 Performance of proposed scheme in terms of BER for $N_t = 4$ and $N_r = 4$, 16, and 32 with BPSK Constellation.

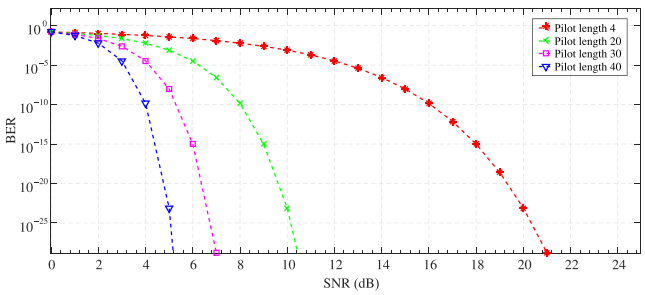

FIGURE 4 Performance of proposed scheme with variable pilot sequence length for fixed $N_t = 4$ and $N_r = 4$

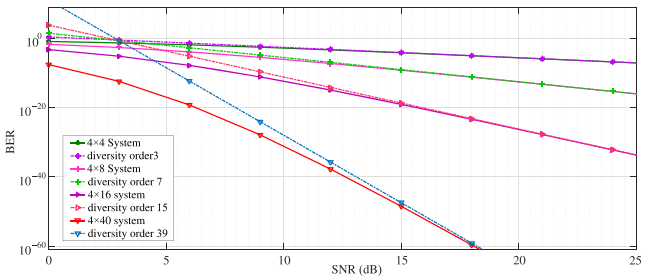

FIGURE 5 Performance of proposed scheme with diversity order, $N_t = 4$ and $N_r = 4$, 8, 16, and 40 with BPSK Constellation.

TABLE 1 Insight of Figure 3.

Type	No. of antennas ($N_t \times N_r$)	BER	Estimation error (%)
Analytical	4×4	0.1466	0.27
Simulated	4×4	0.147	
Analytical	4×8	0.005181	0.038
Simulated	4×8	0.005183	
Analytical	4×16	$1.525 \times 10^{(-5)}$	0.0196
Simulated	4×16	$1.5254 \times 10^{(-5)}$	
Analytical	4×32	$1.9 \times 10^{(-12)}$	0.00275
Simulated	4×32	$1.999945 \times 10^{(-12)}$	

impossible. Multiple copies of the same signal are sent through different independent channels, and the fading experienced by each copy of the signal varies. This ensures that at least one copy of the data signal experiences less fading. Thus, the possibility of receiving the transmitted data increases. As a result, this increases the reliability of the system. This process of transmitting multiple copies of a signal is defined as diversity [28, 29]. A signal can be transmitted by antenna diversity using multiple transmitting antennas (transmit diversity) and/or multiple receiving antennas (reception diversity) in wireless transmission. To analyze the behavior of a communication system at a very high SNR, the diversity order becomes an important parameter. By substituting very high values of SNR in (49), we obtain

$$Q_K \approx \sum_{s=1}^{3} \frac{\psi_s}{(\psi_s \upsilon \mu_i)^{(N_r-1)}} = \frac{\zeta}{(\mu_i)^{(d_o)}}, \tag{50}$$

where ζ is a constant and d_o is the diversity order of the proposed scheme. The diversity order of the proposed system is $N_r - 1$.

4 | RESULTS

Figure 3 depicts a simulated and analytical plot of BER versus SNR with $N_t = 4$ and $N_r = 4$,16, and 32 with binary phase shift key (BPSK) constellation in MATLAB. Because the length of pilot sequences and data symbol vectors are directly proportional to each other and the minimum length of the pilot sequence is the number of receiving antennas, for simplicity, the pilot sequences are considered $\boldsymbol{\rho}_1 = [1000]$, $\boldsymbol{\rho}_2 = [0100]$,$\boldsymbol{\rho}_3 = [0010]$ and $\boldsymbol{\rho}_4 = [0001]$ for $N_t = 4$ and $N_r = 4$ case. For $N_t = 4$ and $N_r = 16$, the pilot sequences are $\boldsymbol{\rho}_1 = [1000100010001000]$, $\boldsymbol{\rho}_2 = [0100010001000100]$, $\boldsymbol{\rho}_3 = [0010001000100010]$ and $\boldsymbol{\rho}_4 = [0001000100010001]$.

The data symbol vectors are obtained from the BPSK constellation. Figure 3 shows that the performance of the system is improved as the number of receiving antennas (N_r) increases. The plot of BPSK with $N_t = 4, N_r = 16$ shows that gain is approximately 19.5 dB better than $N_t = 4, N_r = 4$ at BER $= 10^{-2}$. In a study [12], data symbols are detected with known channels under STTS. The difference between the analytic and simulated results is 2 dB [12]. Figure 4 shows the effect of the length of a pilot sequence on the performance of the proposed scheme when the numbers of transmitting and receiving antennas are constant. For simplicity, $N_t = 4, N_r = 4$, and pilot sequence lengths are 4, 20, 30, and 40. From Figure 4, for pilot sequence lengths 4 and 16, the SNR is 8 and 16 dB at BER $= 10^{-10}$, respectively. This means that for BER $= 10^{-10}$, the plot is 8 dB better. Figure 4 shows that the BER decreases as the pilot sequence length increases. Figure 5 shows the plot of diversity order with analytical 4×4, 4×8, 4×16, and 4×40 systems. This scheme leads to the diversity order of $(N_r - 1)$, that is, three for four receiving antennas. The values of analytical and simulated BERs and estimation error (%) of Figure 3 have been provided in Table 1.

5 | CONCLUSION

Channel coefficients were estimated using orthogonal pilot sequences under the proposed STTS. Data symbol vectors were detected using the estimated channel gain. Figure 3 shows that performance improves as the number of receiving antennas increases. The BER decreased with an increase in the length of a pilot sequence (Figure 4). The obtained diversity order of the proposed scheme was less by one than the number of receiving antennas. According to the analysis results, the minimum length of a pilot sequence was the number of receiving antennas. The proposed scheme is specifically useful for base station-base station communication in colocated MIMO

systems with an even number of transmitting antennas. The expression of the SER was developed using the MGF. OSTBCs work with more than two antennas, whereas the proposed STTS works with four or more antennas. The decoding rate with OSTBCs [44] with four transmitting antennas is 5/8, i.e., 0.625, whereas that with STTS, under the same condition, is 8/16, that is, 0.5. The decoding complexity increases as the data rate increases in OSTBCs. However, this is not the case with STTS because the concept of space null is used.

ORCID

Pratibha Rani https://orcid.org/0000-0002-2831-5333

REFERENCES

1. L. H. Brandenburg and A. D. Wyner, *Capacity of the Gaussian channel with nemory: The multivariate case*, Bell Syst. Tech. J. **53** (1974), no. 5, 745–778.
2. E. Bjornson, J. Hoydis, and L. Sanguinetti, *Massive MIMO has unlimited capacity*, IEEE Trans. Wireless Commun. **17** (2018), no. 1, 574–590.
3. T. L. Marzetta, *Noncooperative cellular wireless with unlimited numbers of base station antennas*, IEEE Trans. Wireless Commun. **9** (2010), no. 11, 3590–3600.
4. M. Sakai, K. Kamohara, H. Iura, H. Nishimoto, K. Ishioka, Y. Murata, M. Yamamoto, A. Okazaki, N. Nonaka, S. Suyama, J. Mashino, A. Okamura, and Y. Okumura, *Experimental field trials on MU-MIMO transmissions for high SHF wide-band massive MIMO in 5G*, IEEE Trans. Wireless Commun. **19** (2020), no. 4, 2196–2207.
5. H. Wang, J. Wang, and J. Fang, *Grant-free massive connectivity in massive MIMO systems: Collocated versus cell-free*, IEEE Wireless Commun. Lett. **10** (2021), no. 3, 634–638.
6. C. V. Nahum, L. De Novoa Martins Pinto, V. B. Tavares, P. Batista, S. Lins, N. Linder, and A. Klautau, *Testbed for 5G connected artificial intelligence on virtualized networks*, IEEE Access **8** (2020), 223202–223213.
7. H. N. Qureshi, M. Manalastas, S. M. A. Zaidi, A. Imran, and M. O. Al Kalaa, *Service level agreements for 5G and beyond: Overview, challenges and enablers of 5G-healthcare systems*, IEEE Access **9** (2021), 1044–1061.
8. M. Säily, C. B. Estevan, J. J. Gimenez, F. Tesema, W. Guo, D. Gomez-Barquero, and D. Mi, *5G radio access network architecture for terrestrial broadcast services*, IEEE Trans. Broadcast. **66** (2020), no. 2, 404–415.
9. E. G. Larsson, O. Edfors, F. Tufvesson, and T. L. Marzetta, *Massive MIMO for next generation wireless systems*, IEEE Commun. Mag. **52** (2014), no. 2, 186–195.
10. R. W. Heath and A. J. Paulraj, *Switching between diversity and multiplexing in MIMO systems*, IEEE Trans. Commun. **53** (2005), no. 6, 962–972.
11. L. Jacobs and M. Moeneclaey, *Effect of MMSE channel estimation on BER performance of orthogonal space-time block codes in Rayleigh fading channels*, IEEE Trans. Commun. **57** (2009), no. 5, 1242–1245.
12. P. Rani, M. K. Arti, P. K. Dimri, and M. Vashishath, *Pilot based space-time transmission scheme for large MIMO system*, (6th International Conference on Signal Processing and Integrated Networks, Noida, India), 2019. https://doi.org/10.1109/SPIN.2019.8711644
13. C. Karnna, S. Udomsiri, and S. Phrompichai, *Channel estimation based on pilot signal and iterative method for TDD based massive MIMO systems*, (International Electrical Engineering Congress, Khon Kaen, Thailand), 2022, pp. 1–4.
14. A. Misso, M. Kissaka, and B. Maiseli, *Exploring pilot assignment methods for pilot contamination mitigation in massive MIMO systems*, Cogent Eng. **7** (2020). https://doi.org/10.1080/23311916.2020.1831126
15. L. Su and C. Yang, *Fractional frequency reuse aided pilot decontamination for massive MIMO systems*, (IEEE 81st Vehicular Technology Conference, Glasgow, UK), 2015, pp. 1–6.
16. J. Ma, C. Liang, C. Xu, and L. Ping, *On orthogonal and superimposed pilot schemes in massive MIMO noma systems*, IEEE J. Selected Areas Commun. **35** (2017), no. 12, 2696–2707.
17. I. Jarin and S. P. Majumdar, *Performance evaluation of MLD and ZFE in a MIMO ODFM system impaired by carrier frequency offset, phase noise and timing jitter*, (IEEE International Conference on Telecommunications and Photonics, Dhaka, Bangladesh), 2017, pp. 122–126.
18. E. Bjrnson, E. G. Larsson, and M. Debbah, *Massive MIMO for maximal spectral efficiency: How many users and pilots should be allocated?* IEEE Trans. Wireless Commun. **15** (2016), no. 2, 1293–1308.
19. Z. Zhao, Z. Chen, and Y. Liu, *Cell sectorization-based pilot assignment scheme in massive MIMO systems*, (Wireless Telecommunications Symposium, New York, USA), 2015, pp. 1–5.
20. X. Zhu, Z. Wang, L. Dai, and C. Qian, *Smart pilot assignment for massive MIMO*, IEEE Commun. Lett. **19** (2015), no. 9, 1644–1647.
21. V. Mishra, P. K. Tripathi, P. Rana, and H. D. Joshi, *Performance analysis of comb type pilot aided channel estimation in OFDM with different pilot sequences*, (Tenth International Conference on Wireless and Optical Communications Networks, Bhopal, India), 2013, pp. 1–5.
22. V. B. Niranjane and D. B. Bhoyar, *Performance analysis of different channel estimation techniques*, (International Conference on Recent Trends in Information Technology, Chennai, India), 2011, pp. 74–78.
23. K. Kim, J. Lee, and J. Choi, *Deep learning based pilot allocation scheme (DL-PAS) for 5G massive MIMO system*, IEEE Commun. Lett. **22** (2018), no. 4, 828–831.
24. C.-K. Wen, W.-T. Shih, and S. Jin, *Deep learning for massive MIMO CSI feedback*, IEEE Wireless Commun. Lett. **7** (2018), no. 5, 748–751.
25. V. Tarokh, H. Jafarkhani, and A. R. Calderbank, *Space-time block codes from orthogonal designs*, IEEE Trans. Inform. Theory **45** (1999), no. 5. https://doi.org/10.1109/18.771146
26. V. Tarokh, N. Seshadri, S. Member, and A. R. Calderbank, *Space-time codes for high data rate wireless communication: Performance criterion and code construction*. IEEE Trans. Inform. Theory **44** (1998), no. 2. https://doi.org/10.1109/18.661517
27. G. Ganesan and P. Stoica, *Space-time block codes: A maximum SNR approach*. IEEE Trans. Inform. Theory **47**, (2001). https://doi.org/10.1109/18.923754
28. M. K. Arti and S. K. Jindal, *OSTBC Transmission in shadowed-Rician land mobile satellite links*, IEEE Trans. Veh. Technol. **65** (2016), no. 7, 5771–5777.

29. A. M.k. and M. R. Bhatnagar, *Performance analysis of two-way AF MIMO relaying of OSTBCs with imperfect channel gains*, IEEE Trans. Veh. Technol. **63** (2014), no. 8, 4118–4124.
30. M. K. Arti, *OSTBC Transmission in large MIMO systems*, IEEE Commun. Lett. **20** (2016), no. 11, 2308–2311.
31. T. L. Marzetta, J. Jose, A. Ashikhmin, and S. Vishwanath, *Pilot contamination and precoding in multi-cell TDD systems*, IEEE Trans. Wireless Commun. **10** (2014), no. 8, 2640–2651.
32. H. Mohammadghasemi, M. F. Sabahi, and A. R. Forouzan, *Pilot-decontamination in massive MIMO systems using interference alignment*, IEEE Commun. Lett. **24** (2020), no. 3, 672–675.
33. M. M. Shurman, O. Banimelhem, D. A. Al-Lafi, and S. J. Al-Zaro, *Pilot contamination mitigation in massive MIMO-based 5G wireless communication networks*, (9th International Conference on Information and Communication Systems, Irbid Jordan), 2018, pp. 192–197.
34. G. Chu, K. Niu, W. Wu, and F. Yang, *MGF-based analysis of spectrum sensing over K-μ fading channels for 5G cognitive networks*, IEEE Access **6** (2018), 78650–78658.
35. J. G. Proakis and M. Salehi, *Digital Communications*, 5th ed., McGraw Hill, 2007.
36. X. Wang, Moment generating function of uncertain variable, (Proceedings - 2018 10th International Conference on Intelligent Human-Machine Systems and Cybernetics, Hangzhow, China), 2018, pp. 129–132.
37. L. Hong and A. Garcia Armada, *Bit error rate performance of MIMO MMSE receivers in correlated Rayleigh flat-fading channels*, IEEE Trans. Veh. Technol. **60** (2011), no. 1, 313–317.
38. N. Kim and H. Park, *Bit error performance of convolutional coded MIMO system with linear MMSE receiver*, IEEE Trans. Wireless Commun. **8** (2009), no. 7, 3420–3424.
39. S. Park and D. Yoon, *An alternative expression for the symbol-error probability of MPSK in the presence of I/Q unbalance*, IEEE Trans. Commun. **52** (2004), no. 12, 2079–2081.
40. M. K. Arti, *A Space-time transmission scheme for large MIMO systems*, IEEE Wirelss Commun. Lett. **7** (2018), no. 1. https://doi.org/10.1109/LWC.2017.2753800
41. A. Jaiswal, M. Abaza, M. R. Bhatnagar, and V. K. Jain, *An investigation of performance and diversity property of optical space shift keying-based FSO-MIMO system*, IEEE Trans. Commun. **66** (2018), no. 9, 4028–4042.
42. I. M. R. I.S. Gradshteyn, *Table of Integrals, Series, and Product*, Seventh Ed *Edited by* D. Z. Alan Jeffrey, Boston, 2007.
43. M. K. Simon and M. S. Alouini, *Digital Communication Over Fading Channels*, Seventh, John Wiley, Hoboken, New Jersey, 2005.
44. X.-B. Liang, *Orthogonal designs with maximal rates*, IEEE Trans. Inform. Theory **49** (2003), no. 10, 2468–2503.

AUTHOR BIOGRAPHIES

Pratibha Rani received her BTech Degree in electronics and communication engineering from Maharaja Agrasen Institute of Technology, Rohini, New Delhi, India, and MTech Degree in electronics and communication engineering from JCBUST, YMCA, Faridabad, Haryana, India. She is currently pursuing her PhD in wireless communication in the electronics engineering department at J.C. Bose University of Science and Technology, YMCA, Faridabad, Haryana, India. Her research interests include signal processing, massive multiple-input multiple-output systems, decoding, channel estimation, and error statistics.

Arti M.K. received her BE Degree in electronics engineering from Madan Mohan Malviya Engineering College, Gorakhpur, India, and MTech Degree in communications engineering and PhD in wireless communications from the Department of Electrical Engineering, IIT Delhi, New Delhi, India. She is currently a Professor with the Department of Electronics and Communications Engineering, NSUT East Campus (AIACTR), New Delhi. Her research interests include signal processing for multiple-input-multiple-output systems, cooperative communications, and satellite communications.

Pradeep Kumar Dimri is currently working as Professor and Chairperson of the Electronics Engineering Department in JC Bose University of Science and Technology, YMCA Faridabad (India). He received his BE from Jamia Milia Islamia, Delhi, and MTech and PhD from M.D. University, Rohtak (India). He has more than 30 years of academic and industrial experience. His current research area includes Embedded Systems, MIMO Communication, and Power Electronics.

How to cite this article: P. Rani, A. M.K., and P. K. Dimri, *Channel estimation and detection with space–time transmission scheme in colocated multiple-input and multiple-output system*, ETRI Journal **45** (2023), 952–962. DOI 10.4218/etrij.2022-0243